Geomorphology 371 (2020) 107422

Contents lists available at ScienceDirect

Geomorphology

journal homepage: www.elsevier.com/locate/geomorph

Morphometric evolution of Everest region debris-covered glaciers

Owen King [a,*], Andy G.D. Turner [b], Duncan J. Quincey [b], Jonathan L. Carrivick [b]

[a] School of Geography and Sustainable Development, University of St Andrews, St Andrews, Scotland, United Kingdom of Great Britain and Northern Ireland
[b] School of Geography and water@leeds, University of Leeds, West Yorkshire LS2 9JT, England, United Kingdom of Great Britain and Northern Ireland

ARTICLE INFO

Article history:
Received 3 July 2020
Received in revised form 4 September 2020
Accepted 4 September 2020
Available online 10 September 2020

Keywords:
Debris-covered glacier
Glacier metrics
Structure from motion
Glacier surface topography
Glacier surface relief

ABSTRACT

Debris-covered glaciers in the central Himalaya have now experienced several decades of sustained ice loss, manifested predominantly in glacier surface lowering. In particular, glacier surfaces of low longitudinal gradient and low ice surface velocity have developed locally complex surface topographies and undergone profound changes in supraglacial hydrology. In this study we examine the development of complex ice surface topography across six debris-covered glaciers in the Everest region over the last four decades via a new metric of glacier surface relief applied to Digital Elevation Models (DEMs). We focus in on Khumbu Glacier, and use fine spatial and temporal resolution DEMs covering a period of 28 months to quantify the contemporary contribution of ice cliff and supraglacial pond expansion to overall mass loss from stagnant areas of ice. On the broader scale, we find three common long-term changes in glacier surface topography, (1) glacier-wide expansion of high relief topography in response to ice cliff and supraglacial pond network evolution, (2) up-glacier expansion of high local relief zones that may be caused by differential sub-debris melt beneath thin debris, and (3) increase in glacier surface relief proximal to glacier termini caused by supraglacial stream incision where linked proglacial-supraglacial hydrological networks exist. Overall, we contend that these topographic measurements will be important for understanding glacier surface water storage and also the energy balance of a debris-covered glacier surface, both of which could exacerbate future ice loss and downstream meltwater supply.

1. Introduction

The Himalaya contains the greatest terrestrial ice mass outside the Polar Regions, comprising more than 18,000 glaciers (RGI Consortium, 2017). Glaciers in the Himalaya have now been losing mass for at least the last five decades and the rate of ice loss has increased towards the present day (Bolch et al., 2019; King et al., 2019; Maurer et al., 2019). There is much spatial variability in the current mass loss rate of Himalayan glaciers, with local climate (Mukherjee et al., 2018), glacier terminus type (Brun et al., 2019; King et al., 2019) and glacier surface debris cover (Brun et al., 2019; King et al., 2019) all influencing ice loss rates. Between 14 and 18% of the total glacier surface area is covered by supraglacial debris (Kääb et al., 2012), with debris cover patterns varying considerably between catchments, and across individual glacier surfaces, although it is predominantly situated in glacier ablation zones. Further expansion of debris cover is still expected for many Himalayan glaciers in the coming decades despite the already widespread debris mantle on many glaciers (Herreid and Pellicciotti, 2020).

The presence of debris cover complicates the response of a glacier to climate change (Rowan et al., 2015; Anderson and Anderson, 2016) because it influences the downward flux of energy that is available for melt at the glacier surface. Melt can either be enhanced by a thin layer of surface debris that preferentially absorbs and transmits incident solar radiation, due to its lower albedo, to ice beneath; or melt can be inhibited by a thick layer of debris that stores and re-emits incoming energy with only a small portion reaching the ice surface below (Østrem, 1959; Nicholson and Benn, 2006). Consequently, many debris-covered glaciers persist at relatively low altitudes no longer occupied by clean ice glaciers (Rowan et al., 2015).

Spatial variability in melt rates leads to the development of a complex surface topography that is not commonly found on clean-ice glaciers. Where debris cover is thick, ice loss is focused at exposed ice cliffs and with supraglacial pond growth (Sakai et al., 2002; Watson et al., 2017b). Ponds and cliffs typically occupy a very small total area of debris-covered glacier ablation zones, but account for a substantial portion of ice loss. Thompson et al. (2016) estimated that ponds and cliffs cover 5% of the debris-covered portion of Ngozumpa, but account for 40% of melt over the same area. Brun et al. (2018) found that 7–8% of the surface of Changri Nup glacier was composed of ice cliffs which accounted for 23 ± 5% of the total ablation over the period November 2015 to November 2017. Similarly, Immerzeel et al. (2014) estimated that cliffs and ponds covered ~8% of their study area on Lirung glacier but accounted for 24% of total ice melt over their study period.

* Corresponding author.
E-mail address: ogak1@st-andrews.ac.uk (O. King).

https://doi.org/10.1016/j.geomorph.2020.107422

The development of a complex glacier surface topography on debris-covered ice can also heavily impact supraglacial hydrology (Watson et al., 2017a, 2017b; Miles et al., 2019). Differential melt, ice cliff backwasting and supraglacial pond development creates more accommodation space for the storage of supraglacial meltwater, thus modulating freshwater runoff and water quality (Irvine-Fynn et al., 2017). Should a supraglacial pond network persist, particularly over glacier surfaces of low slope and low surface velocity, pond coalescence and ultimately glacial lake development may occur (Quincey et al., 2007; King et al., 2018). The presence of lakes at Himalayan glacier margins has amplified terminus retreat and ice mass loss rates (King et al., 2019). Floods from glacial lakes can travel many hundreds of kilometres downstream and have been responsible for the great loss of life in the Himalaya (Carrivick and Tweed, 2016; Miles et al., 2018).

Despite the importance of glacier surface topography as a control on melt, supraglacial hydrology, hazard development and ultimately meltwater yield, there remains little knowledge of how debris-covered glacier surface topography evolves over decadal timescales, particularly during periods of rapid ice loss. In this study we therefore aim to examine the topographic evolution of debris-covered glacier surfaces in the Everest region of the Himalaya over the last 32 years by analysing two sets of fine-resolution Digital Elevation Models (DEMs). Specifically, we derived glacier surface elevation change data through DEM differencing to examine broad-scale patterns of glacier thinning. We then developed a new surface metric that examines the local variability in glacier surface topography to quantify the impact of long-term ice loss on glacier surface morphometry in the region. We also examine changes in the glacier surface at a high (annual) temporal resolution using DEMs derived from Structure from Motion - Multiview Stereo (SfM-MVS) that reveal the dominant melt processes operating at the surface of one of the debris-covered glaciers in our sample. Using these datasets, we identify the processes driving glacier surface topography change, and examine how their spatial extent and concentration has altered in recent decades.

2. Study site

We focus our study on six glaciers located in the Everest region of the Nepal Himalaya (Fig. 1, Table 1). The study of long-term glacier change is the Everest region is facilitated by the historical surveys of Mt. Everest and its surrounding valleys originally intended to aid mountaineering expeditions in the region. Some of these historical datasets have been combined with more contemporary data to reveal long term ice loss from many of the region's glaciers since the 1960s (Bolch et al., 2011; Nuimura et al., 2012), which has been driven by increasing air temperature, particularly in winter months, and weak precipitation since at least the early 1990s (Salerno et al., 2015).

Khumbu Glacier is the largest glacier we study and originates in the Western Cwn below Mt. Everest. The glacier initially flows west, before turning to flow south below its icefall. In 2011, 24% of the surface of Khumbu Glacier was covered by debris, whereas in 1962, 15% of the glacier was covered by a debris layer (Thakuri et al., 2014). The debris layer increases in thickness down-glacier, from a few cm near the base of its icefall, to more than 2 m near its terminus (Rowan et al., 2015; Rounce et al., 2018). An extensive network of supraglacial ponds and ice cliffs exists over the lower 6 km of the glacier (Watson et al., 2016). Between November 2009 and February, Khumbu Glacier gained >99,000 m^2 of ponded area (Watson et al., 2016), and the number of ice cliffs present in its ablation zone increased from 436 to 520 (Watson et al., 2017a). Bolch et al. (2011) showed increasing surface lowering rates over the lower reaches of the glacier using a time series of DEMs spanning the period 1962–2007 (-0.34 ± 0.19 m a^{-1} from 1962 to 1970 versus -0.79 ± 0.52 m a^{-1} from 2002 to 2007). The moderate resolution of their DEMs precluded the attribution of enhanced surface lowering to a developing network of cliffs and ponds, but the pattern of surface lowering they show is similar to that caused by cliff and pond expansion that has been documented on the nearby Ngozumpa Glacier (c.f., Thompson et al., 2016).

Lhotse Nup and Lhotse Glaciers flow south from the foot of the Lhotse/Nuptse Massif (8516 & 7861 m a.s.l., respectively). These glaciers are 5.1 and 7.1 km in length and show substantial debris cover that has also expanded in recent decades. Thakuri et al. (2014) estimated debris cover extent to be 31% and 36%, respectively for these two glaciers in 1962, and 40% and 42% in 2011. A large proportion of their ice mass input likely comes from avalanching (Benn and Lehmkuhl, 2000). Watson et al. (2016) documented slight increases in ponded area on Lhotse and Lhotse Nup Glaciers (expansion of 25,341 m^2 and 7524 m^2) between November 2009 and February 2015. Both of these glaciers hosted a similar number of ice cliffs in 2009 (Lhotse- 299, Lhotse Nup- 59) and 2015 (Lhotse- 293, Lhotse Nup- 71) (Watson et al., 2017a).

Lhotse Shar and Imja Glaciers coalesce before terminating into Imja Tsho - a lake that has been expanding since the early 1960s (Somos-Valenzuela et al., 2014; Thakuri et al., 2016). Thakuri et al. (2014) treated the two glaciers as one system, and showed a slight (2%) increase in debris cover area between 1962 and 2011. Watson et al. (2016, 2017a) documented a decrease in the number of ice cliffs (459 to 289 on Lhotse Shar, 168 to 122 on Imja) and total ponded area ($-56{,}634$ m^2 and -6050 m^2) for Lhotse Shar and Imja glaciers between 2009 and 2015. King et al. (2018) showed increased velocities over the lower reaches of Lhotse Shar Glacier over the period 2000–2015 and suggested that the expansion of Imja Tsho may be influencing glacier dynamics.

Ama Dablam Glacier flows north from the eastern flank of Ama Dablam (6812 m a.s.l.). Unlike the glaciers on the opposing valley side (Lhotse, Lhotse Nup and Nuptse Glaciers), Ama Dablam Glacier flows down from a broad, clean ice accumulation zone that feeds a short (4.3 km) debris-covered ablation zone. This debris-covered tongue comprised 26% of total glacier area in 2011 (Thakuri et al., 2014). This section of the glacier has thinned since the 1970s (Bolch et al., 2011).

3. Methods

3.1. DEM generation

Our analyses are based on DEMs generated using three different approaches: stereo photogrammetry using aerial photographs (hereafter AP-DEM), stereo photogrammetry using WorldView satellite imagery (hereafter WV-DEM), and Structure from Motion (SfM) with Multi-View Stereo (MVS) (hereafter SfM-DEM) using close range terrestrial photographs. WV-DEMs were generated from several pairs of 0.5 m resolution WorldView-1 and WorldView-2 imagery using the Surface Extraction with Triangular Irregular Network (TIN)-based Search-Space Minimization (SETSM) algorithm described by Noh and Howat (2015). The WorldView scenes were captured on the 21st March 2016 over the Imja Valley. The WV-DEM covering the Khumbu valley is a composite of two DEMs, one derived from imagery acquired on the 31st Jan 2015 and one acquired from imagery acquired on the 2nd February 2015. We assumed that no substantial surface elevation change occurred in the Khumbu valley during the two-day gap between the acquisition dates and mosaicked the two WV-DEMs. The SETSM algorithm used to generate the WV-DEMs uses only the Rational Polynomial Coefficients (RPCs) as geometric constraints, the geolocation accuracy of which is 5 m (Noh and Howat, 2015). RPCs are updated by the SETSM algorithm to increase the geolocation accuracy of DEMs to ± 4 m in X, Y and Z directions. WV-DEMs were generated at 2 m ground resolution.

SfM-MVS DEMs were generated following three detailed terrestrial photographic surveys of the ablation zone of the Khumbu Glacier, from the icefall in the middle of the glacier to the terminus in October 2015, May 2016 and May 2017. These surveys were completed by traversing moraine ridges and elevated routes along valley sides and taking photos of the surface of the glacier and its lateral moraines at regular intervals (approximately every 30 m). All three surveys were

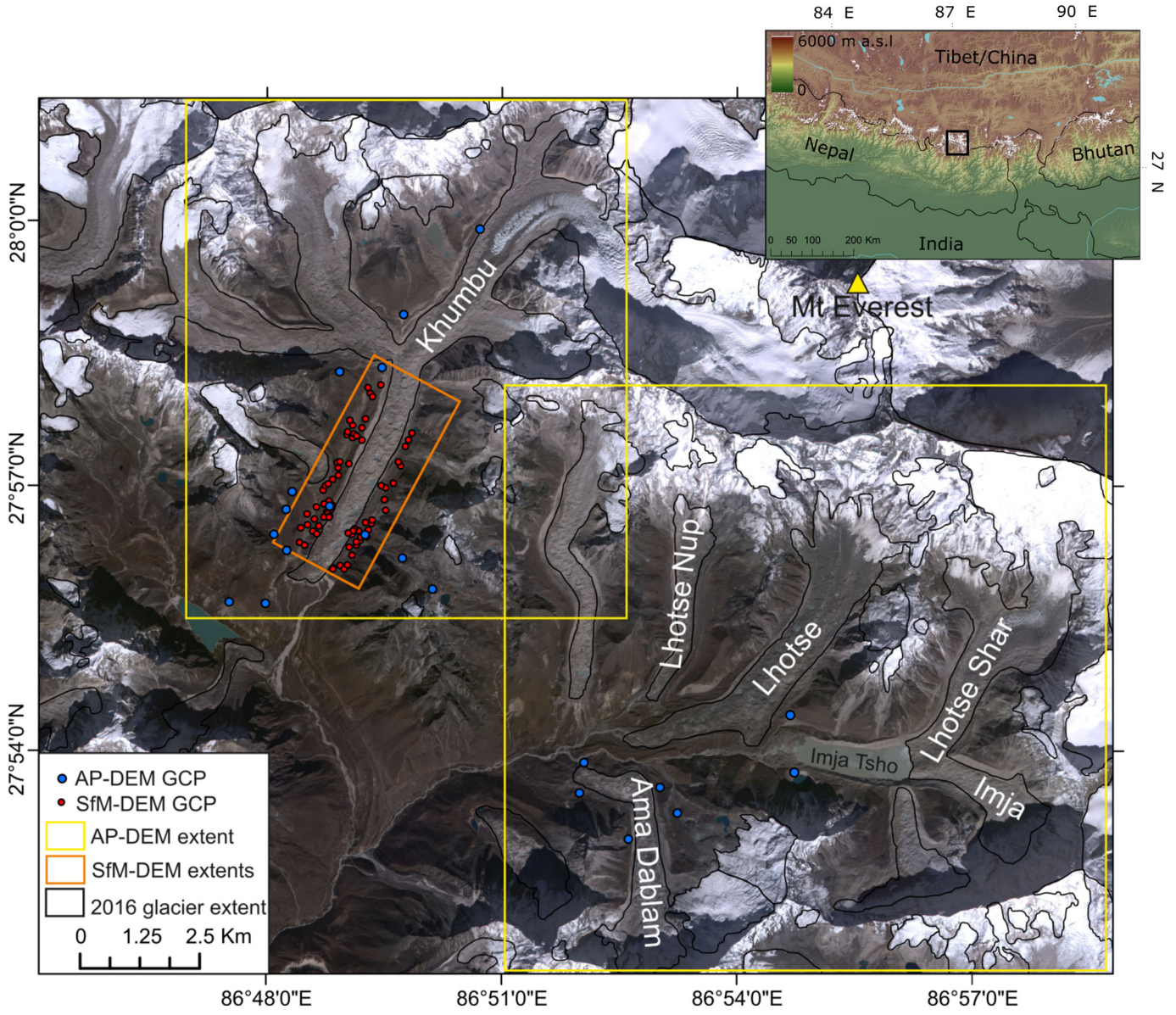

Fig. 1. The six glaciers we focus on in this study, and the extent of the DEM datasets. WV-DEM coverage is complete for the entire study area and is therefore not shown on the figure. Background image is a RapidEye scene captured in April 2015. Inset map shows the location of the Everest region in a broader context.

conducted using the same survey route, and all contained a very similar number of photographs (~1300 in each survey). We used Agisoft Photoscan (version 1.3.4) to carry out the processing steps required in a standard SfM-MVS workflow (e.g. Smith et al., 2016). Camera alignment and sparse point cloud generation were carried out and only points with a reprojection error of <1.5 were retained. Field-derived Ground Control Points (GCPs) (see Section 3.2) were identified and placed in photographs from each epoch (October 2015, May 2016 and May 2017). The mean GCP Root Mean Square error (RMSE) was 0.25 m ($n = 25$) in the October 2015 survey, 0.26 m ($n = 27$) in the May 2016 survey, and 0.25 m ($n = 25$) in the May 2017 survey. Dense point clouds were produced using PhotoScan's MVS algorithm and were cleaned manually to remove obvious blunders. We used the Topographic Point Cloud Analysis Toolkit (ToPCAT) (Brasington et al., 2012)

Table 1
Attributes of glaciers studied. Glacier ID and elevation information extracted from RGI V6.0 (RGI Consortium, 2017).

Glacier ID	Glacier name	Length (km)	Area (km^2)	Min elev. (m)	Max elev. (m)	Range (m)	Debris cover (%)
G086917E27925N	Lhotse	7.1	6.9	4821	6082	1261	42
G086820E27978N	Khumbu	15.7	39.5	4915	8062	3147	24
G086949E27913N	Lhotse Shar	6.5	7.01	5021	7998	2977	27
G086949E27913N	Imja	3.71	8.29	5019	8000	2981	35
G086889E27929N	Lhotse Nup	5.1	3.89	4979	5470	491	40
G086882E27875N	Ama Dablam	6.25	5.51	4761	6170	1409	26

to decimate and rasterise the resulting point cloud, setting a minimum point density of 10/m^2 to produce a 2 m resolution DEM from each time period.

The AP-DEM was derived from fine resolution (0.5 m ground resolution) aerial photographs acquired in 1984 using a Wild RC-10 camera (Washburn, 1989). We used 7 images from the Bradford Washburn aerial photo set, purchased from Swissphoto and scanned at 1693 dpi using the original diapositives. DEM processing was carried out using PCI Geomatica within a frame camera geometric model setup and 2 m DEMs were produced, matching the resolution of the WV & SfM DEMs. Aerial photograph pairs were processed separately for the Khumbu and Imja valleys due to insufficient overlap between image pairs at the edges of each valley for a single composite DEM to be generated. The outer limits of each of the AP-DEMs fell over Nuptse Glacier, and this glacier has not been included in further analyses because of poor data quality in the peripheral areas of the two AP-DEMs. Seventeen evenly spread GCPs were used in the Khumbu valley AP-DEM generation, and seven in the Imja valley AP-DEM generation (Fig. 1).

3.2. Ground control

The geolocation of our AP-DEM and SfM DEMs was fixed using an extensive set of GCPs collected in the Khumbu and Imja valleys. We collected 70 spot height measurements of stable features (mostly large boulders) easily distinguished in both the terrestrial photographic surveys from each epoch, and the aerial photographs (Fig. 1). We used two Leica GS10 differential GPS (dGPS) units to collect GCPs. One dGPS unit was deployed as a temporary base station over the duration of the October 2015 survey, with the other used as a rover to collect GCPs. Each GCP was occupied in static mode for a minimum of 10 min. We used simultaneous position, phase and ephemeris data from the permanent Syangboche dGPS base station (approximately 20 km from the Khumbu) to resolve the position of our temporary base station at the Khumbu, and then used this temporary base station location as a fixed reference against which we could adjust the location of our rover-measured GCPs. All dGPS data processing was completed using Leica Geoffice software, and the mean 3-D positional uncertainty of the 70 GCPs used in AP-DEM and SfM-DEM processing was 5.1 mm.

3.3. DEM coregistration and bias removal

The generation of DEMs from imagery acquired by different sensors and through different approaches (with or without ground control data) resulted in some geolocation inconsistencies between the different DEMs. Initial differencing of the AP-DEMs against the WV-DEMs revealed a misalignment between these DEM sets. We eliminated co-registration error between the AP-DEM and WV-DEMs by following the methods of Nuth and Kääb (2011). We used the WV-DEM as the master DEM during the co-registration process because of its greater coverage of the study area compared to SfM-DEMs. The mean and standard deviation of off-glacier AP-DEM-WV-DEM elevation differences was −0.66 & 8.36 m for the Imja valley, and −0.39 & 7.14 m for the Khumbu valley following co-registration.

3.4. Topographic classification of glacier surfaces

Features of complex local topography are ubiquitous on debris-covered glaciers. Ice cliff complexes are easily distinguished from the surrounding, undulating topography of the glacier surface, and from supraglacial ponds, by their contrasting slope or vertical relief. DEMs of sufficiently fine resolution to capture small-scale changes in surface topography can therefore be interrogated to distinguish such features and the distribution and density of such features examined in both space and time. The extent of such features can also be quantified from optical imagery but may be time consuming because of the requirement of manual digitisation (in the case of ice cliffs – Watson et al., 2017a), and may be somewhat complicated by spatially homogenous spectral characteristics of the debris mantled surface.

To identify different glacier surface features from our fine resolution topographic datasets, we developed a Statistical Measure of Relief (hereafter SMR) metric to summarise the local relief of a subset region of the glacier. The SMR metric is a sum of the negative elevation differences within a specified diameter circular window, relative to a central cell within that window; it follows therefore that areas of high relief are represented by high SMR values, whereas areas of low relief are represented by low SMR values. We produced this metric using 4 cell (8 m diameter), 8 cell (16 m diameter) and 16 cell (32 m diameter) windows, and assessed which produced the most realistic estimate of local relief associated with ice cliff features, and which was able to distinguish the most accurate extent of such features, using a the photographs used to generate SfM models as reference (Supplementary Table 1). The 8 cell window was deemed most appropriate for identifying features with sharp changes in relief (ice cliffs), as well as more gentle breaks in glacier surface topography. The 4 cell window was too constrained to identify features of moderate relief (reclined ice cliffs), and the 16 cell window yielded estimates of surface relief that were an order of magnitude too large to be representative of individual ice cliffs (1000s m of relief), as well as smoothing features of high relief beyond their actual extent (Fig. 2). Our subsequent analyses therefore focused on metric grids produced using an 8 cell window on both the 1984 and 2015/16 DEMs, examples of which are given in Fig. 3.

To assess the variability of glacier surface characteristics in both space and time, we split the SMR metric into categories, each of which represented a different topographic classification of the glacier surface. Categories were defined for the supraglacial environments that represented particular thresholds of negative elevation differences. Based on field observations and SfM survey photographs, and detailed satellite image interpretation, SMR values of <75 m were interpreted as representing gently undulating, debris-covered or, near some glacier termini, soil mantled areas; values of 76–125 m were identified as representing debris-covered glacier surfaces of sufficient relief to allow debris slumping; values of 126–175 m were identified as representing ice cliff flanks, and values of 176 m or greater were identified to be associated with ice cliff faces. Herein, SMR metric values of <75 m are referred to as SMR_{75}, 76–125 m as SMR_{75-125}, 126–175 as $SMR_{125-175}$ and > 176 m as SMR_{175}. The total area occupied by different classes was calculated for 500 m distance bins along each glacier and compared for the AP- and WV-DEMs. Supraglacial ponds were removed from analyses using pond extent data from Watson et al. (2016), which were coincident with our study period.

3.5. Additional data sources

We combined the fine resolution DEMs and glacier surface metric data with datasets of glacier velocity and supraglacial pond extent generated by Dehecq et al. (2015) and Watson et al. (2016) for the Everest region. Glacier surface velocity data were generated by tracking surface features in a series of Landsat 7 (ETM+) and 8 (OLI) panchromatic images (see Dehecq et al., 2015 for more details) over the period 2013–2015. Multiple velocity fields from this period were combined using a median value for each pixel to give an average velocity field that coincided with the date of our contemporary DEM sets. The supraglacial pond extent datasets of Watson et al. (2016) were generated using a combination of Object Based Image Analysis (OBIA) and manual digitisation of WorldView 1 & 2, GeoEye, Pleiades and QuickBird imagery. The pond extents of Watson et al. (2016) cover several time periods, and we used the most recent pond extents (2013–2015) for each glacier in our study. We also generated supraglacial pond extents from the 1984 aerial photographs following the same OBIA approach as Watson et al. (2016).

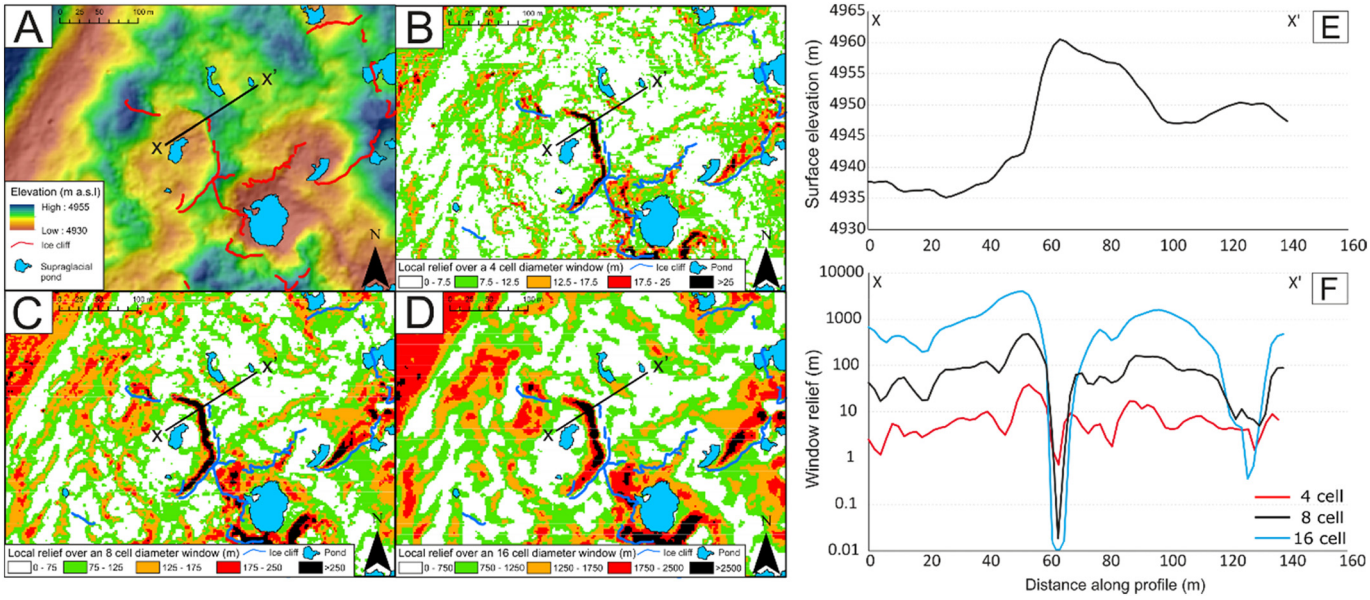

Fig. 2. SMR values derived over a subset area of the debris covered ablation zone of the Khumbu glacier (A) considering windows of different cell diameters (B-D). The local relief along a transect (X-X') through a prominent ice cliff (E) considering different window diameters is also shown (F).

3.6. Uncertainty

We estimated the uncertainty associated with glacier surface elevation change by deriving the standard error in 100 m altitudinal bands of off-glacier elevation difference data (Bolch et al., 2011). We followed King et al. (2019) and weighted error estimates by glacier hypsometry (glacier area split into 100 m altitudinal bands) to better represent the spatial variability of uncertainty. The uncertainty associated with surface elevation change over clean-ice areas is higher (Table 2) than over debris-covered ice because debris-free glacier surfaces are found at a higher elevation in the region, where topographic shading or low image contrast caused by fresh snow cover may cause blunders in DEM generation. Still, our estimated uncertainty remains well below the rate of surface elevation change on-glacier due to the high-resolution of the aerial and satellite images we have used.

To better understand the impact of DEM blunders on our topographic metric data we examined the differences in the total area of different metric classes over off-glacier areas which we presumed remained stable over our study period. By comparing stable terrain areas, we are also able to test how reliably the SMR algorithm replicates the vertical relief of topography reconstructed from different data sources in our DEMs. We limited our comparison of off-glacier metric areas to slopes of less than 30° to avoid the comparison of erroneous data caused by topographic shading and areas of natural slope instability. There was a 2.74% difference in the total area of the SMR_{75} between the AP- & WV-DEMs; a − 0.07% difference in the total area of $SMR_{75–125}$; a − 3.30% difference in the total area of $SMR_{125–175}$, and a 0.64% difference in the total area of $SMR_{>175}$. These values are well below the changes detected in the area covered by different metric classes on glacier. Finally, we estimated the uncertainty associated with our supraglacial pond and debris extent mapping using a plus or minus one-pixel perimeter buffer (Watson et al., 2016). The orthoimages generated alongside the AP-DEM were 1.5 m resolution and the RapidEye scene used is 6.5 m resolution.

4. Results

4.1. Multi-decadal surface elevation change

Differencing of the AP-DEM and WV-DEMs illustrates substantial ice loss from each glacier over the 32 year study period (Fig. 4). Surface lowering rates varied depending on the presence of a debris mantle (Table 2) and throughout the different elevation ranges of each glacier (Fig. 4). Land-terminating glaciers (Khumbu, Lhotse, Lhotse Nup and Ama Dablam) showed most substantial surface lowering several kilometres up-glacier (Figs. 4 & 5). In the case of Khumbu Glacier, maximum surface lowering (~75 m) occurred close to the clean ice debris-covered transition zone below the location of Everest base camp (EBC on Fig. 4). Surface lowering was slight (10–20 m) immediately below the Khumbu icefall, and minimal in the terminus region (mean of −5.7 m within lowermost 1 km). In the case of Lhotse, Ama Dablam, and Lhotse Nup Glaciers, surface lowering was most substantial (means of −17.2, −24.2 and − 16.1 m within 1 km of the debris-clean ice transition, maximum of ~ −65 m on each glacier) immediately below the steep headwall and avalanche debris cones present on each glacier (Fig. 4). These glaciers did show slight surface lowering in their terminal regions (mean of −11.4, −12.9 & −8.2 m within 1 km of glacier termini). Five of the six glaciers showed surface lowering in clean ice areas above the extent of debris cover, and only Khumbu Glacier showed any positive elevation change, close to Everest Base Camp. Ice surface elevation increases here were 5–10 m over an area where a large supraglacial pond developed (also noted by Bolch et al., 2011), which has since drained and its basin closed.

The lake-terminating Lhotse Shar - Imja Glacier complex shows a reversed surface lowering gradient when compared with land-terminating glaciers (Fig. 5). The surface of this glacier lowered most (~85 m) over the area through which Imja Tsho expanded over the study period. The surface lowering measured here comprises the elevation change between the glacier surface and the new lake level, with considerably more ice being lost below the waterline than is captured here. Surface lowering rates on the Lhotse Shar - Imja Glacier complex decreased slightly in an up-glacier direction, but overall were the most substantial out of all the glaciers in our sample (Table 2). Surface lowering over debris-covered ice exceeded that over clean-ice areas for all of the glaciers in our sample (Table 2).

4.2. Topographic classification & decadal evolution of glacier surfaces

The contribution of each topographic class to the total glacier surface area varied substantially with distance up-glacier on each of the glaciers we assessed. In general, the surfaces of Khumbu, Lhotse Nup, Lhotse and Ama Dablam glaciers showed lowest relief close to glacier termini, but

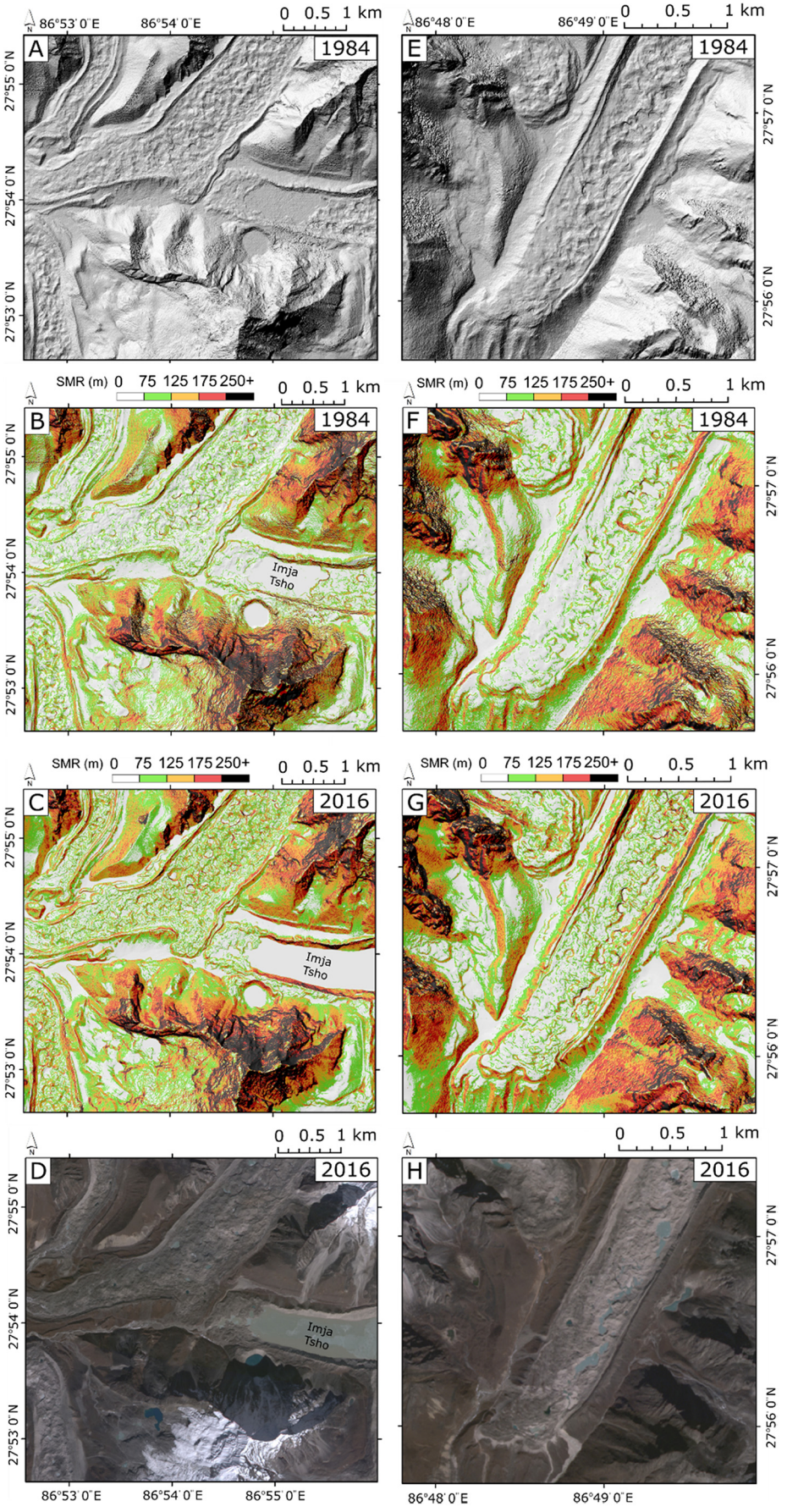

Fig. 3. Hillshade of the AP-DEM (A, E), SMR metric datasets for 1984 (B, F) and 2016 (C, G) and RapidEye imagery (D, H) over the termini of Lhotse and Khumbu glaciers.

Table 2
Changes in the debris-covered area of the ablation zone of each glacier, along with estimates of total surface lowering (dh), and surface lowering rates (dh/dt), for clean and debris-covered ice over the study period.

Glacier	1984 debris-covered area (km^2)	2016 debris-covered area (km^2)	Δ debris cover area (km^2)	Mean debris-covered area dh (m)	Mean debris-covered area dh/dt ($m\ a^{-1}$)	Mean clean ice dh (m)	Mean clean ice area dh/dt ($m\ a^{-1}$)	Δ pond area (m^2)
Khumbu	8.20 ± 0.06	8.52 ± 0.20	0.32 ± 0.13	−29.86 ± 2.84	−0.93 ± 0.09	−28.80 ± 2.91	−0.90 ± 0.09	98,469 ± 13,785
Lhotse Nup	1.66 ± 0.02	1.72 ± 0.05	0.06 ± 0.03	−12.87 ± 1.96	−0.40 ± 0.06	−10.50 ± 3.14	−0.33 ± 0.10	18,651 ± 4289
Lhotse	6.02 ± 0.03	6.30 ± 0.09	0.28 ± 0.06	−17.88 ± 2.22	−0.56 ± 0.06	−6.24 ± 3.14	−0.20 ± 0.10	35,368 ± 5328
Lhotse Shar	6.73 ± 0.03	6.04 ± 0.08	0.69 ± 0.06	−31.30 ± 2.65	−0.97 ± 0.06	−5.68 ± 4.77	−0.17 ± 0.14	10,943 ± 2298
Imja	1.23 ± 0.02	1.47 ± 0.05	0.24 ± 0.04	−32.26 ± 1.24	−1.00 ± 0.06	−16.22 ± 2.37	−0.51 ± 0.07	−2655 ± 345
Ama Dablam	2.51 ± 0.02	2.69 ± 0.06	0.18 ± 0.04	−21.70 ± 1.36	−0.68 ± 0.04	−12.07 ± 5.81	−0.38 ± 0.18	−15,233 ± 2132

much greater relief further up-glacier. Within ~1 km of their termini, >50% of these glacier surfaces comprised SMR_{75} in both time periods (Figs. 6 and 7). The area covered by SMR_{75} decreased to as little as 35%, 3–5 km from the terminus of each of these glaciers. In both time periods, the proportion of glacier surfaces covered by $SMR_{75–125}$ to SMR_{175} peaked in the middle reaches of Khumbu, Lhotse Nup, Lhotse and Ama Dablam Glaciers (Figs. 6 and 7), but were generally limited to less than 40% of the total glacier surface area. $SMR_{175,}$ the metric

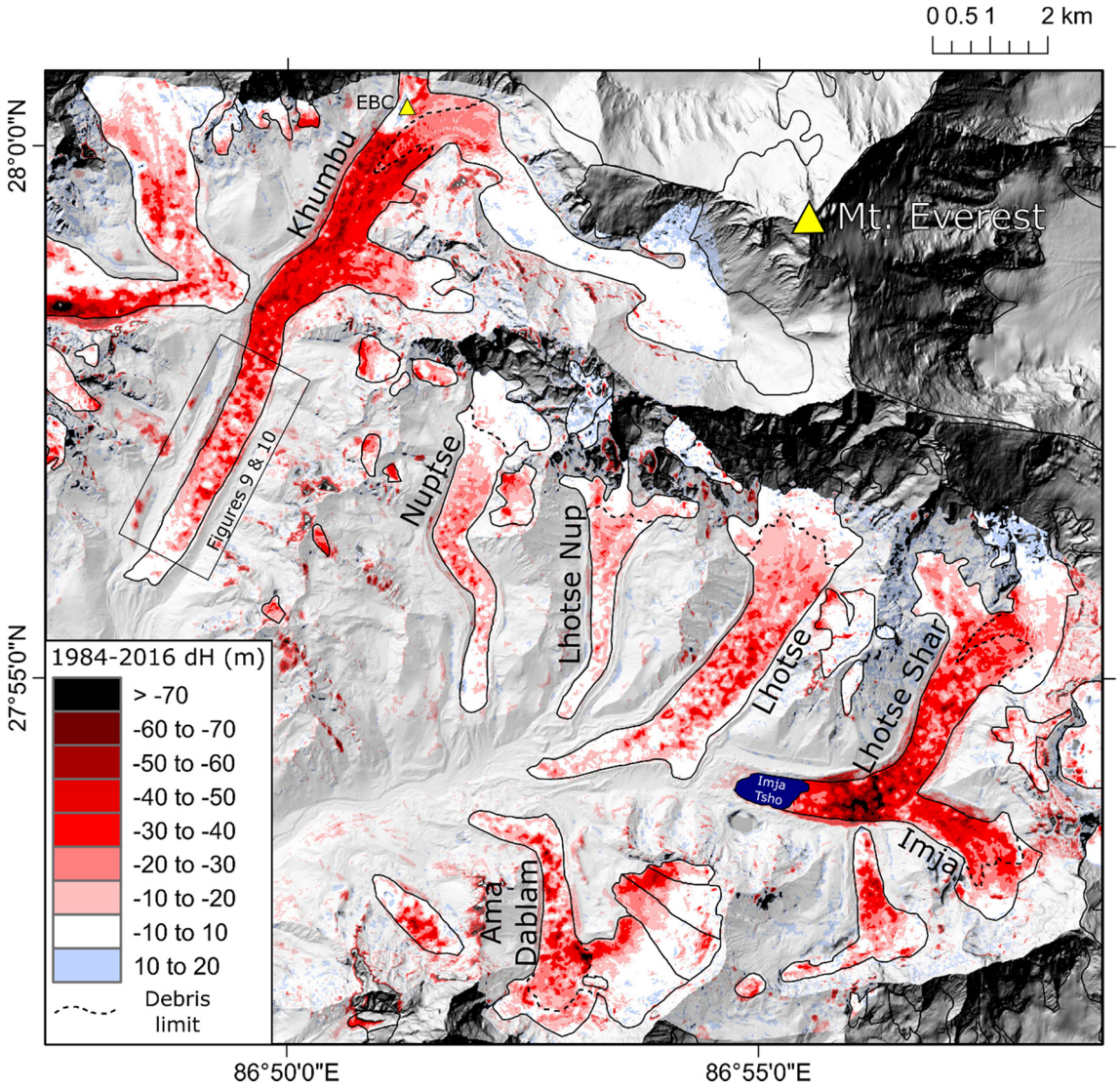

Fig. 4. Difference in surface elevation between the AP-DEM (1984) and WV-DEMs (2015/16). Inset shows the subset area covered by SfM-MVS DEMs in Figs. 9 & 10. Glacier outlines are based on the RGI 6.0 which have been modified to reflect the 1984 glacier extent in aerial orthophotos.

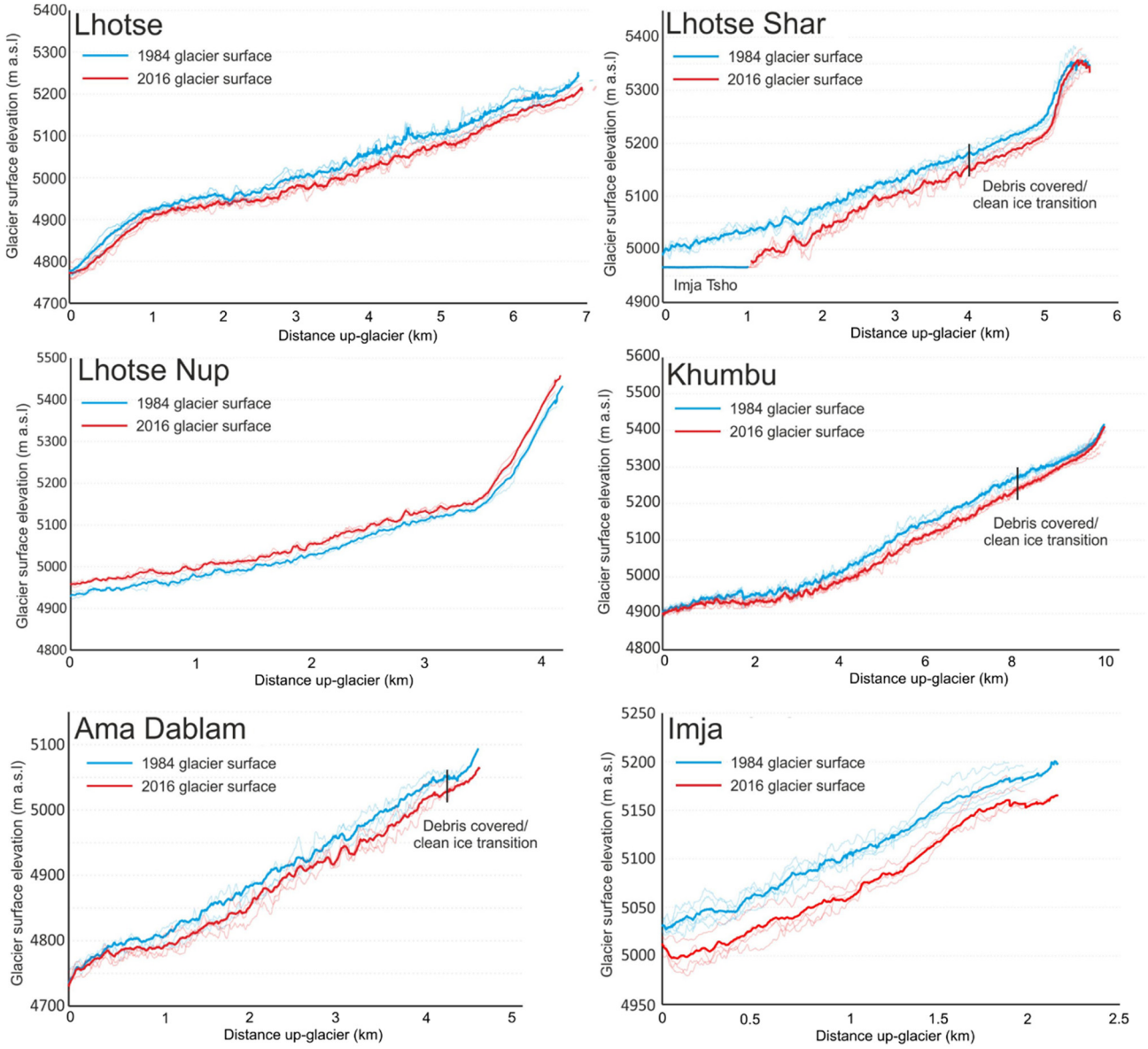

Fig. 5. Glacier surface elevation profiles taken from AP- and WV-DEMs. Semi-transparent lines are flow-parallel surface elevation profiles spaced 100 m apart across each glaciers surface, and the opaque elevation profiles represent a mean of flowline-parallel profiles. Locations of debris-covered- clean ice transition are also shown. Lhotse, Lhotse Nup and Imja glaciers have fully debris-covered ablation zones.

class associated with ice cliffs, generally accounted for <10% of glacier area on all four of these glaciers but did cover the greatest area in the middle reaches of each glacier.

In contrast to the other four glaciers, the proportion of the surface of Lhotse Shar and Imja Glaciers covered by SMR_{75} increased up-glacier, thus surface relief decreased up-glacier (Fig. 8). The percentage of glacier area covered by $SMR_{75–125}$ to SMR_{175} generally decreased with distance from the termini of Lhotse Shar and Imja Glaciers (Fig. 8).

Substantial changes occurred in the surface topography of all the glaciers we assessed between 1984 and 2015/16. At a broad scale, there is clear evolution of the glacier surfaces towards much greater vertical relief. The patterns and magnitude of changes in surface topography were similar for the four land-terminating, debris-covered glaciers we examined. Khumbu Glacier showed a substantial reduction in the area covered by SMR_{75} over the study period (Fig. 6). Over the debris-covered glacier surface, the area of this class reduced by 22%. The greatest reductions in SMR_{75} occurred between 4 and 7 km up-glacier on Khumbu Glacier. Concomitant increases in $SMR_{75–125}$ to SMR_{175} occurred in the lower reaches of Khumbu Glacier (Fig. 6), with the most substantial increases occurring >4.5 km up-glacier. The surfaces of Ama Dablam, Lhotse Nup and Lhotse glaciers evolved in similar ways to that of Khumbu Glacier (Fig. 6). The proportion of these glacier surfaces made up of SMR_{75} reduced by 20, 23, and 24%, respectively over the study period, with the largest reductions occurring substantially up-glacier from their termini. Again, increases in $SMR_{75–125}$ to SMR_{175} occurred where the greatest reductions in the total area of low-relief topography occurred on these glaciers. We note that large reductions (20–30%) in SMR_{75} also occurred over the lowermost 2 km of Lhotse glacier, which does not have a pronounced terminal moraine, with substantial increases in the area of $SMR_{75–125}$ occurring over this area. The area covered by SMR_{175} barely changed over the lower reaches of Lhotse glacier between 1984 and 2016 (Fig. 6).

The lake-terminating Lhotse Shar and Imja glaciers also developed predominantly rougher surfaces over the study period (Fig. 7), but changes in surface topography seem more evenly distributed along each of these glaciers ablation zones. The area covered by SMR_{75} reduced by 26% on Lhotse Shar glacier and by 27% on Imja glacier over the full study period (1984–2016).

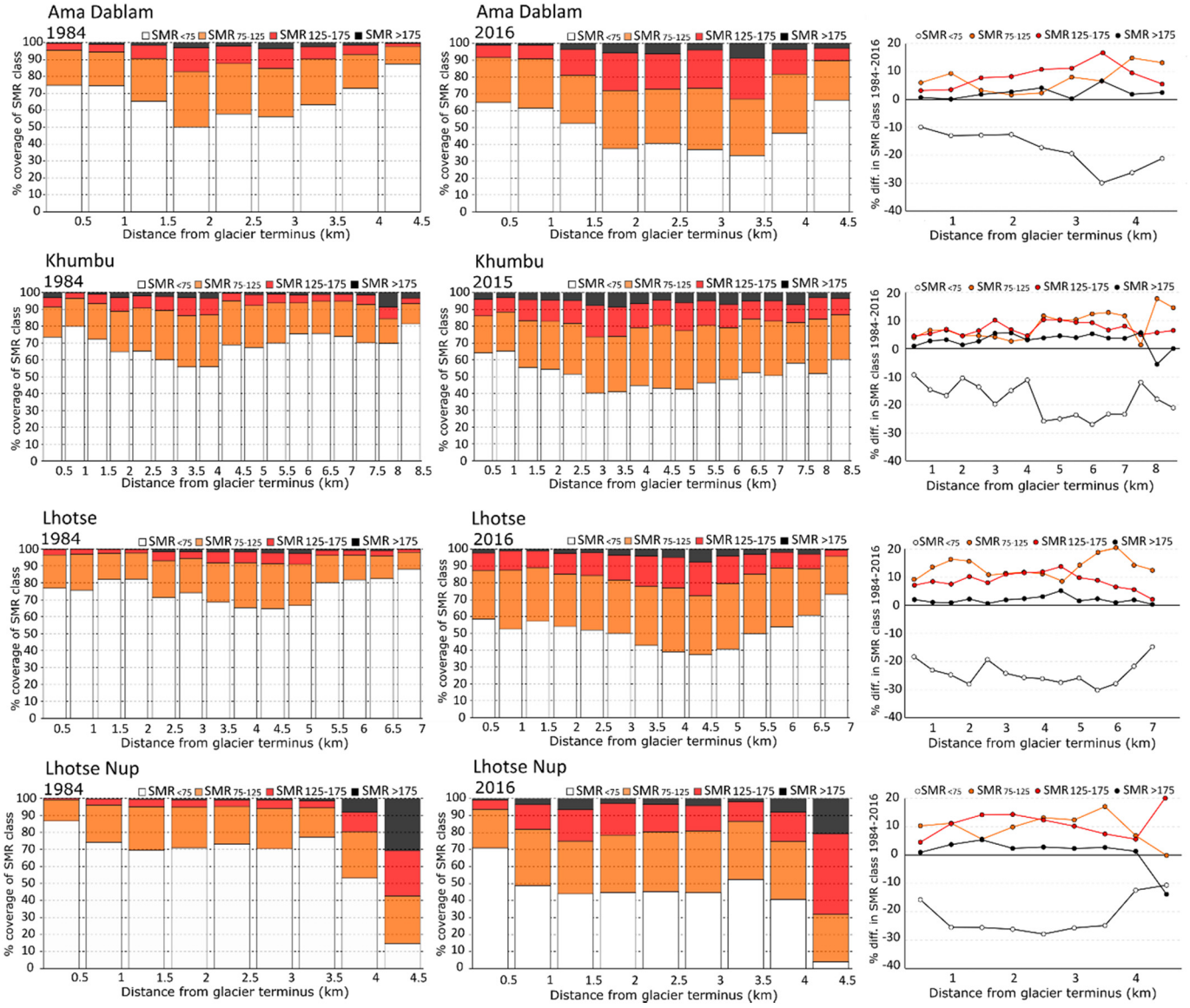

Fig. 6. Percentage of glacier surface area made up of different classes of topography distinguished by the sum of negative elevation differences in a local (8 pixel) area for Ama Dablam, Khumbu and Lhotse and Lhotse Nup glaciers over the period 1984–2015/16. SMR_{75} represents gently undulating, debris-covered glacier surfaces, $SMR_{75–125}$ represents debris-covered areas of sufficient slope to allow debris slumping, $SMR_{125–175}$ represents ice cliff flanks & SMR_{175} represents ice cliff faces.

4.3. Supraglacial pond evolution

Total supraglacial pond area increased on four of the six glaciers we assessed over the study period (Table 2). The greatest increases in supraglacial pond area occurred over the lowermost 3–4 km of Khumbu and Lhotse Nup Glaciers, and in the middle reaches of Lhotse Glacier (Fig. 7). Total ponded area decreased on Ama Dablam and Imja Glaciers, but pond area also decreased within the lowermost 2.5 km of Lhotse and Lhotse Shar Glaciers termini (Fig. 7). The increases in ponded area on Khumbu and Lhotse Nup Glaciers primarily occurred where glacier surface velocity was low ($<$ ~10 m a^{-1}). There were also increases in the ponded area on parts of these glaciers where surface velocities were $>$ 10 m a^{-1}, and the increases in pond area on Lhotse Glacier also occurred where glacier surface velocity was elevated. Similarly, pond area decreased occurred over areas of Lhotse and Ama Dablam Glaciers that were flowing very slowly ($<$ 10 m a^{-1}), and over parts of Lhotse Shar Glacier that were flowing more actively (~15 m a^{-1}).

4.4. Contemporary ice loss

Differencing of the SfM-DEMs against the WV-DEM (Fig. 9) revealed the contemporary pattern of ice loss from the surface of the Khumbu Glacier from the end of January 2015 to May 2017, the pattern of which contrasts with that derived over the decadal timescale (Fig. 5). We focus our analyses of the SfM-DEM difference data on a subset shown in Fig. 4, because this area is constrained with the best ground control data, and benefits from the best photographic coverage. The SfM-DEMs primarily cover the stagnant portion of the glacier. Surface lowering, and therefore ice loss, was concentrated where supraglacial ponds and ice cliffs expanded over the study period. Using supraglacial pond and ice cliff extents from Watson et al. (2016, 2017a), we calculate that pond expansion and cliff retreat accounted for 35% of ice loss over the period between January and October 2015 despite occupying just 13.2% of the subset area of the glacier. The mean backwasting rate (calculated by dividing the total area of surface lowering associated with each cliff by cliff length) of the ice cliffs present in the subset area

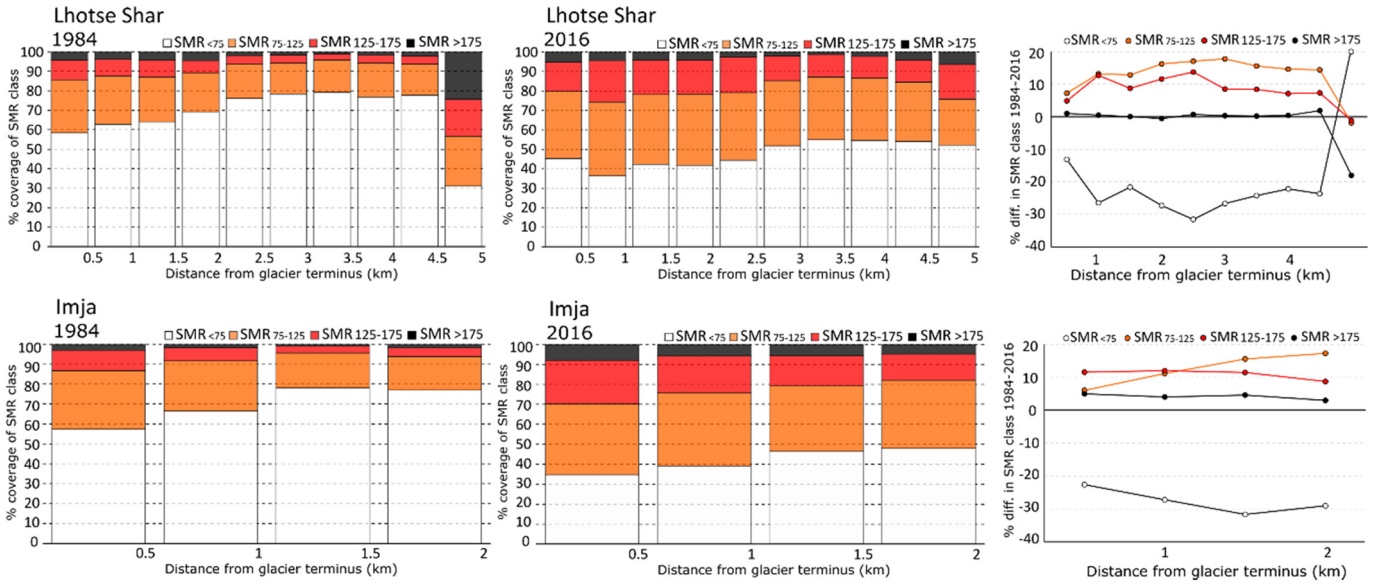

Fig. 7. The percentage of glacier surface area made up of different classes of topography distinguished by the sum of negative elevation differences in a local (8 pixel) area for the lake-terminating Lhotse Shar and Imja glaciers. SMR_{75} represents gently undulating, debris-covered glacier surfaces, $SMR_{75–125}$ represents debris-covered areas of sufficient slope to allow debris slumping, $SMR_{125–175}$ represents ice cliff flanks & SMR_{175} represents ice cliff faces.

shown in Fig. 4 was 13.51 m a^{-1}, ranging from 6.43–18.55 m a^{1}. Cliff expansion affected 8.7% of the glacier surface in the subset area (118,495 m^2 of 1,351,849 m^2 subset) over our 28 month study period. Assuming a temporally consistent rate of cliff expansion in the future would result in a complete turnover of the glacier surface in just under 26 years within this subset region.

The predominance of ice cliff expansion and retreat as the primary source of ice melt in the lower region of Khumbu Glacier (Fig. 9) is also evident in the topographic metric data generated from the WV-DEM (Jan 2015) and 2017 SfM-DEM (Fig. 10). Heavily negative values in the difference between the two SMR metric datasets represent areas where local relief diminished between Jan 2015 and May 2017

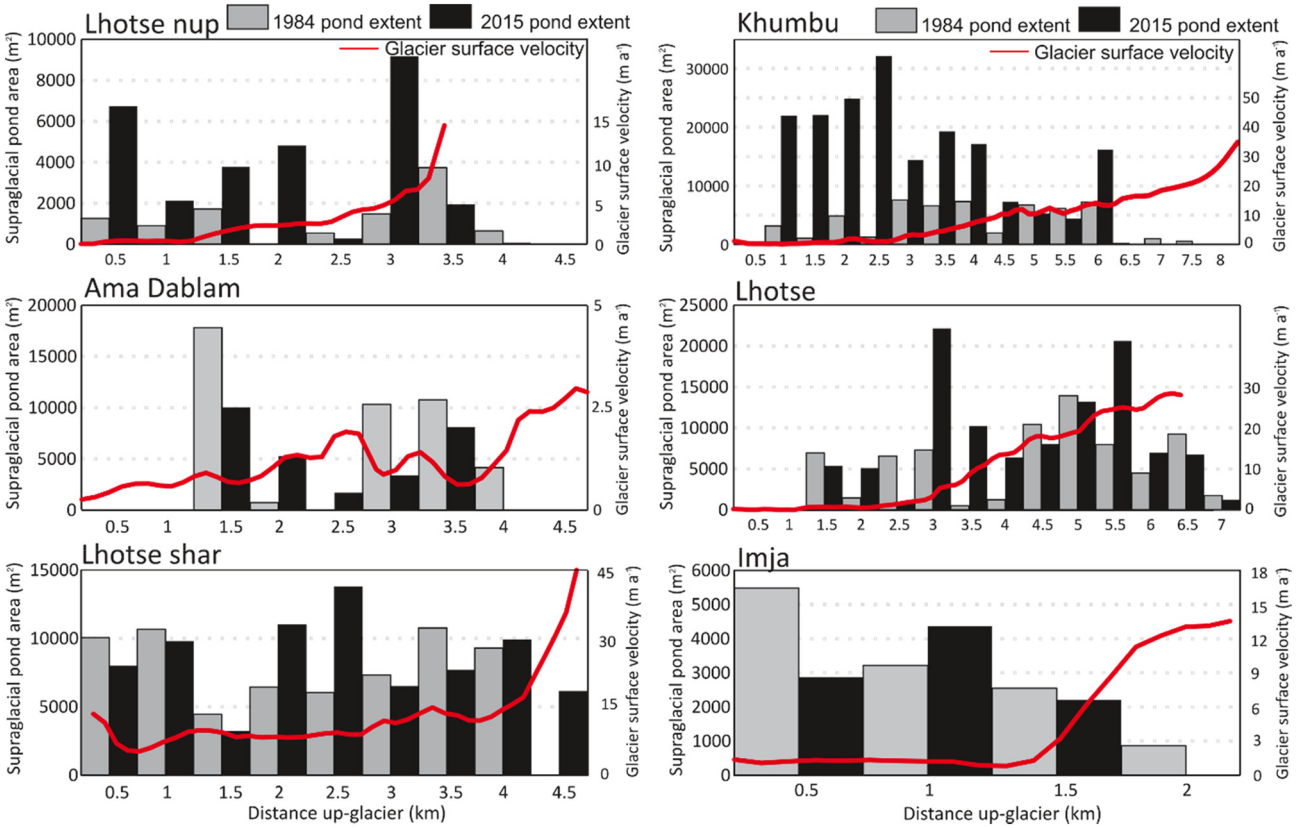

Fig. 8. Supraglacial pond area mapped using the AP-DEM and data from Watson et al. (2016), and glacier surface velocity data from Dehecq et al. (2015).

over the lower part of Khumbu Glacier. These large negative differences are restricted to the former locations of ice cliffs that backwasted over the study period, and to parts of the unstable lateral moraines that slumped or collapsed over the study period. Large positive differences between the two SMR metric datasets indicate areas that developed much more vertical relief over the study period. Such positive differences are again focused where cliff backwasting occurred, or where substantial slumping occurred on lateral moraines, to increase local topographic relief. Isolated, positive differences between the two SMR metric sets are also evident in many areas of the lower Khumbu Glacier (Fig. 10), which represent newly developed areas of localised relief (primarily new ice cliffs). The area of positive differences (values >100 in SMR) was greater (58,810 m^2 Vs 56,434 m^2) than the area of negative differences (values <100) by 4% in this subset of the Khumbu Glacier between Jan 2015 and May 2017, indicating the development of a slightly rougher glacier surface in this subset area overall, even over this relatively short time period.

5. Discussion

Our assessment of fine resolution DEMs of the surface of several debris-covered glaciers has revealed the spatially variable evolution of glacier surface topography over the last three decades in the Everest region of the Central Himalaya. The most spatially extensive changes that are evident in our data are, the 1) glacier-wide increase of high relief zones in association with ice cliff and supraglacial pond network expansion, 2) up-glacier expansion of glacier surface topography of high local relief that may be associated with differential melt beneath expanding but thin surface debris, and 3) increase in glacier surface relief proximal to the glacier terminus, possibly due to supraglacial meltwater channel incision where a linked proglacial-supraglacial hydrological network exists.

5.1. Processes driving topographic evolution

Substantial increases in relief are clearly evident over the lower ablation zones of the land-terminating Khumbu, Lhotse, Lhotse Nup and Ama Dablam glaciers (Figs. 6 and 7). More modest increases in surface relief were also focussed around the clean-ice/debris-covered transition zones of land-terminating glaciers, and around the lower margins of the lake-terminating glaciers.

SfM-MVS DEM differencing (Fig. 9) and multi-temporal surface metric comparisons (Fig. 10) over the lower reaches of Khumbu Glacier pinpoint ice cliff and pond network expansion as being the main contemporary drivers of topographic change here, and it is likely that these mechanisms are also responsible for a large part of the change observed over the last three decades too, given our observations of supraglacial pond expansion since the 1980s (Fig. 8). The SMR class changes between the AP- and WV-DEMs (Figs. 5 & 6) were similar for Khumbu, Lhotse Nup, Lhotse and Ama Dablam glaciers, so it is reasonable to suggest that supraglacial pond and ice cliff expansion has driven topographic change in these glacier ablation zones too.

Supraglacial ponds and associated ice cliffs are prevalent over the lower reaches of debris-covered glaciers in the Everest region because these glaciers typically flow very slowly or are completely stagnant (Bolch et al., 2008; Quincey et al., 2009; Fig. 8) thus little crevassing occurs to aid rerouting or drainage of ponded supraglacial meltwater (Quincey et al., 2009). The multi-decadal surface lowering and ice loss that these glaciers have experienced (Figs. 4 & 5; Bolch et al., 2011) has also reduced their longitudinal surface gradient (King et al., 2018) to a point where supraglacial meltwater drainage is inhibited, thus meltwater ponds readily form. King et al. (2018) measured further slowdown of a number of additional land-terminating glaciers in the Everest region in recent years (2000–2015), as did Dehecq et al.

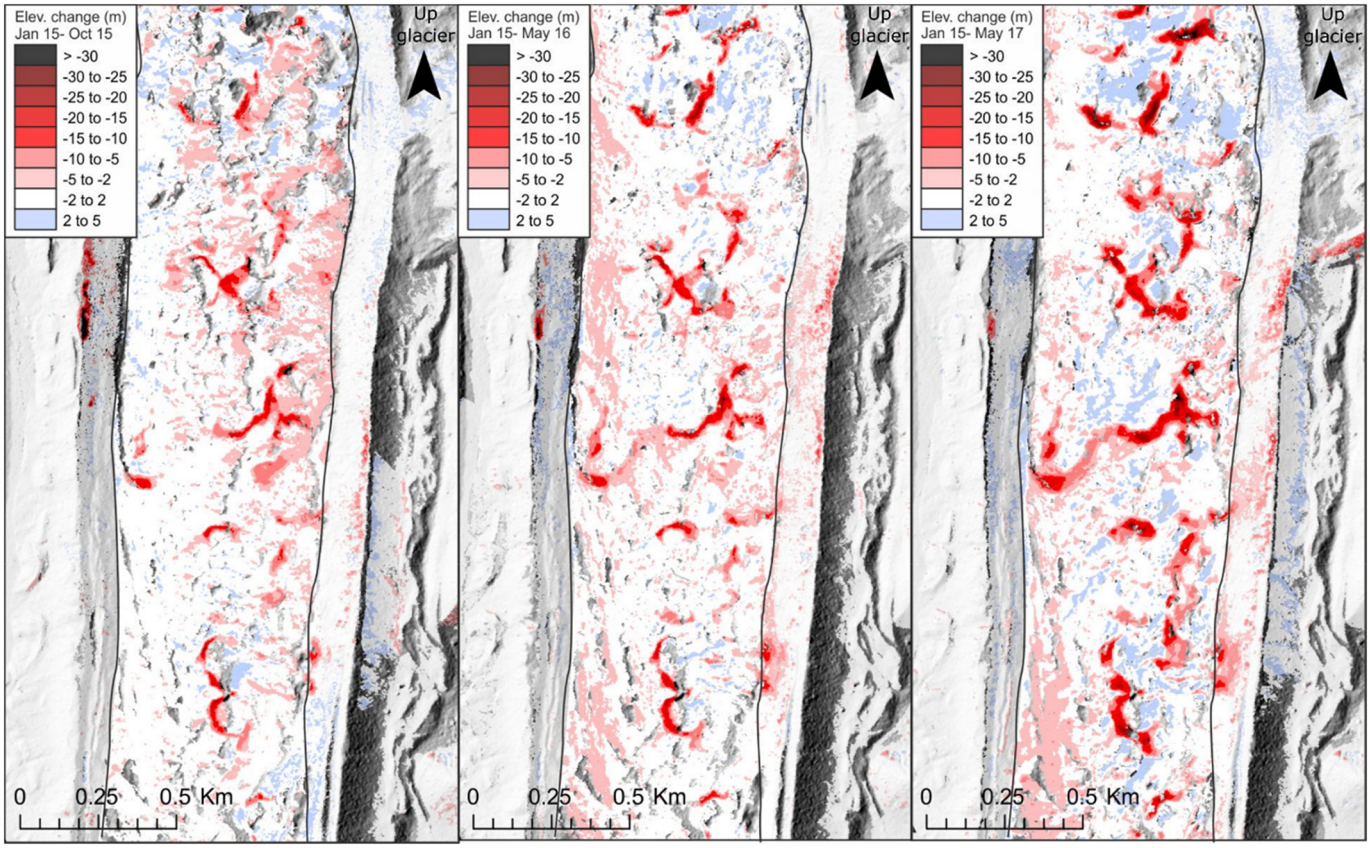

Fig. 9. Difference in surface elevation between the WV-DEM (Jan 2015) and SfM-DEMs acquired in October2015, May 2016 and May 2017.

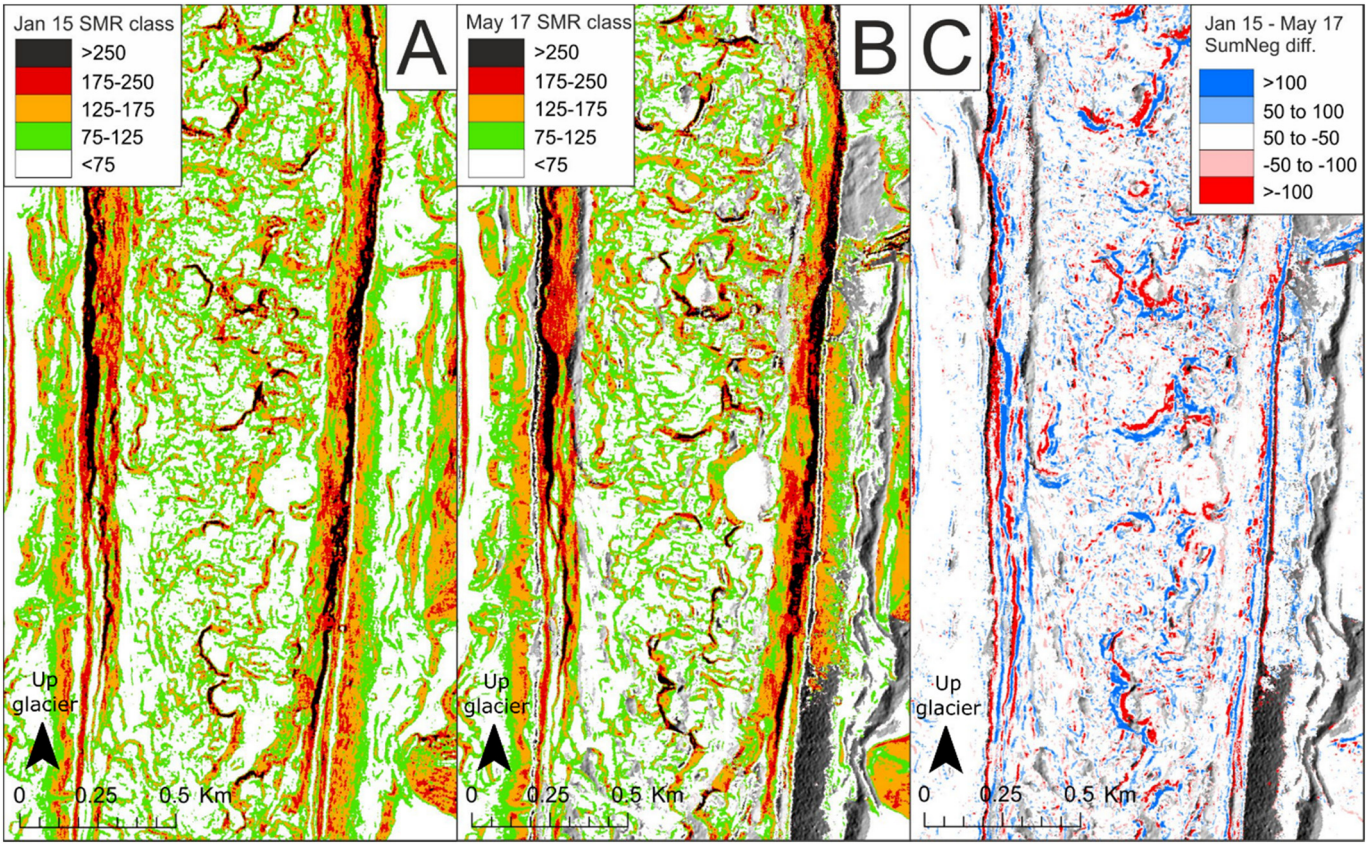

Fig. 10. SMR metric scores generated using the WV-DEM over the lower reaches of Khumbu Glacier in January 2015 (A) and one of the SfM DEMs from May 2017 (B). Panel C shows the difference in metric scores between these two time periods.

(2019) across much of the Himalaya. Similarly, the backwasting rates of ice cliffs (Fig. 9) measured across the ablation zone of Khumbu glacier (mean of 13.51 m a^{-1}, ranging from 6.43–18.55 m a^{1}) and the contribution of ice cliffs and ponds to the overall mass loss budget across this same area (13.2% area covered, 35% ice loss) are comparable to those measured on other Himalayan glaciers (see Thompson et al., 2016 and references within). We would therefore expect that the topographic characteristics of debris-covered glaciers elsewhere in the Everest region and those in a state of negative mass balance outside of the Everest region to have evolved in a similar way to those we have assessed.

A different process may be responsible for the topographic change in areas close to the debris-covered to clean-ice transition zone. Our analyses of AP and WV DEM metrics suggests a glacier surface of greater relief has also developed here on each of the glaciers we studied (Figs. 6 and 7). Glacier flow is typically too high to allow the development of supraglacial pond networks in these areas (Fig. 8) as crevassing promotes the rerouting and drainage of supraglacial meltwater and pond frequency is generally low here (Watson et al., 2016). In this transitional zone debris thicknesses are typically low (Rowan et al., 2015; Rounce et al., 2018), pointing towards spatially variable melt (and associated hummocky surface development) being the dominant driver of the surface changes we observe here.

On Ama Dablam and Lhotse Glaciers, a slightly more pitted surface (Figs. 6 and 7) developed close to each glacier terminus, despite decreases in supraglacial pond extent occurring over the same parts of these glaciers (Fig. 8). This pitted area, reminiscent of thermokarst features described elsewhere within the region (e.g. Haritashya et al., 2018), coincides with slight surface lowering (−11.03 and − 10.62 m means within 1 km of glacier termini), as well as the development of linked supraglacial-proglacial hydrological networks at both sites (Rounce et al., 2017). It is likely, therefore, that the development and subsequent evolution of these supraglacial meltwater channels (e.g. Mölg et al., 2020) is the primary driver of surface roughening in these parts.

5.2. Implications of topographic evolution on glacier melt

The degree of spatial variability in the local relief of a glacier surface can impact heavily on both the energy balance at the surface, and therefore the energy budget available for ice melt, and also on the supraglacial hydrology. A more pitted glacier surface has, by definition, a greater surface area over which radiation and turbulent heat can be absorbed, as well as emitted (Hock, 2005; Quincey et al., 2017; Chambers et al., 2019). In addition, the turbulent fluxes of sensible and latent heat, which are driven by vertical air exchange close to the glacier surface (Hock, 2005), may be substantially different over complex topography (King and Anderson, 1994; Martin and Lejeune, 1998) when compared to smoother, clean ice, particularly where local maxima in air flow exist (Denby and Greuell, 2000). Sakai et al. (2009) showed how wind speeds, and therefore near surface turbulence, peak at ice cliff crests, thus the expanding network of ice cliffs documented by Watson et al. (2017a), and generally more pitted topography we have documented may have driven a greater contribution of the turbulent heat fluxes to the energy balance at the glacier surface, and therefore greater ice melt.

The pitted glacier surface also provides accommodation space in which surface water can pond (Benn et al., 2017; Miles et al., 2016). Watson et al. (2016) showed how supraglacial pond extent increased over the same glaciers in our sample over the period 2000–2015, and Fig. 8 extends this analysis with similar findings for the past three decades. Watson et al. (2016) suggested that the trajectory of pond development on Khumbu glacier may ultimately result in the formation of a large proglacial lake and the surface conditions of other large glaciers in the Everest region may be suitable for comparably widespread

meltwater ponding (Quincey et al., 2007; Benn et al., 2012; King et al., 2018). Irvine-Fynn et al. (2017) showed the buffering effect of the now extensive pond and cliff network on Khumbu Glacier, with >23% of the daily discharge being stored en-route to the terminus. Substantial increases in supraglacial pond area and debris cover have been documented elsewhere in the Everest region, as well as in other regions of the Himalaya (Thakuri et al., 2016; Watson et al., 2016; Miles et al., 2016), playing a potentially pivotal role in capturing and transmitting incident solar radiation to the ice interior. The energy absorbed by supraglacial ponds may enhance ablation either in-situ, further down the linked supraglacial-englacial network, or englacially, where ponds intercept conduits and drain (Miles et al., 2016; Benn et al., 2017). Benn et al. (2017) describe how such subsurface processes can also exert a strong control on the spatial patterns and rates of surface mass loss and therefore glacier surface topography as a whole. As glacier surfaces continue to store water in coming decades, especially as the ice decelerates and surface slopes approach horizontal (King et al., 2018), we would expect further enhancement of the positive feedback between meltwater production, storage, heat absorption and conveyance to the glacier interior.

5.3. Comparison with other studies

Relatively few studies have examined the decadal-scale evolution of the surface characteristics of debris-covered glaciers, mainly due to the paucity of ground observations or high-resolution imagery available to document the prevalence of surface features in times before the modem satellite era. Only two recent studies have examined the evolution of debris-covered glacier surface at temporal and spatial resolutions comparable to ours. First, Mölg et al. (2020) compiled a 140-year long time series of high-resolution DEMs and accompanying orthoimages of Zmuttgletscher, a debris-covered glacier in the Swiss Alps. Secondly, Benn et al. (2017) combined speleological exploration and a time series of satellite images to summarise the supraglacial and englacial drainage system of Ngozumpa Glacier and proposed a conceptual model of its evolution since the Little Ice Age.

Mölg et al. (2020) identified zones of the debris-covered tongue of Zmuttgletscher which could be divided based on their distinctly different topographic characteristics and documented their extent through time in response to changes in the mass balance of the glacier. The high-relief zone on Zmuttgletscher was observed to expand rapidly over the course of a few decades of negative glacier mass balance, which is comparable with our observations of ice cliff and supraglacial pond expansion rates on the glaciers in this study, and also our estimate of the complete turnover of the ablation zone of Khumbu glacier by cliff and pond expansion over two to three decades.

A clear difference between the spatial distribution of topographic features across Zmuttgletscher and the glaciers we have studied is the location of the high-relief zone proximal to the glacier terminus on Zmuttgletscher, whereas the land-terminating glaciers in the Everest region show the greatest concentration of cliffs (Figs. 6 and 7) and ponds (Fig. 8) several km from their termini. The contrasting debris thickness at the termini of Zmuttgletscher and the Himalayan glaciers we studied may explain the location of such high-relief features. Mölg et al. (2019) measured a mean debris thickness of 16.3 cm along transects across the low relief zone of Zmuttgletscher and found a maximum debris thickness of 70 cm here. In contrast, measurements of the debris thickness over the lower reaches of Khumbu Glacier suggest a maximum thickness of ~2 m at its terminus (Nakawo et al., 1986) and the thickness of the debris mantle likely exceeds 20 cm as far as 3.4 km from the terminus (Rounce et al., 2018). Whilst a debris layer of several decimetres may reduce melt by 70–80% when compared to clean ice (Mölg et al., 2019 and references within), only a debris mantle >40 cm would be capable of protecting the ice beneath from ablation entirely (Mattson et al., 1993; Nicholson and Benn, 2006). In the terminal areas of debris-covered glaciers, with a debris mantle several metres in thickness as at Khumbu, spatially variable surface ablation is unlikely to aid the incision of supraglacial meltwater streams to modify the glacier surface topography and topographic change would therefore be more limited.

Benn et al. (2017) examined the evolution of the supraglacial hydrological network on Ngozumpa Glacier, located directly to the west of our study area, and its link to the englacial and subglacial environment. Akin to our observations, Benn et al. (2017) observed the up-glacier expansion of closed topographic depressions and perched ponds between 1964 (observed in Corona imagery) and 2010 and the formation of a large lake at the hydrological base level of the glacier, similar to that currently forming on Khumbu Glacier (Watson et al., 2016). Benn et al. (2017) describe the glacier surface of the upper ablation zone on Ngozumpa Glacier in a similar way to the low relief zone on Zmuttgletscher (Mölg et al., 2020); one that is uninterrupted by crevasses or closed depressions with a system of supraglacial channels. Benn et al. (2017) show how this zone has retreated up-glacier since the 1960s on Ngozumpa glacier. Our surface metric data suggest that similar low relief zones exist close to the debris-covered clean-ice transition zone on Khumbu, Lhotse and Ama Dablam glaciers. On these three glaciers, the coverage of the SMR_{75} metric class is similar high in the ablation zone to the area around glacier termini and the extent of $SMR_{75–125}$, $SMR_{125–175}$ and SMR_{175} classes is low compared to further down glacier (Figs. 6 and 7). Of the glaciers we studied, an extensive supraglacial stream network can only be traced down-glacier on Khumbu Glacier and this stream extends to the former confluence with Changri Nup (Fig. 1) in both 1984 and 2016 (Miles et al., 2019), contrasting with the evolution of the supraglacial hydrological network on Ngozumpa Glacier.

The expansion of high relief zones in response to more negative mass balance, lower glacier flow and high glacier meltwater storage seems ubiquitous on debris-covered glaciers that have been studied in detail and should be expected in regions where similar levels of glacier mass loss have occurred over long time periods. The location of high-relief zones and their associated ablative processes may ultimately be controlled by the thickness of a glacier's debris mantle, which can vary on an individual glacier basis (Rounce et al., 2018).

6. Conclusions

In this study we have used high resolution DEMs to examine the decadal-scale and contemporary evolution of the debris-covered surfaces of six glaciers in the Everest region of the central Himalaya. We derived a metric of glacier surface relief to examine how sustained ice loss has impacted on the characteristics of glacier ablation zones and used a time series of contemporary SfM-MVS derived DEMs to identify the melt processes responsible for driving topographic change. The predominant change in glacier surface topography has been the development of a more pitted surface of greater, local relief, which expanded by ~20%, in response to an increase in the extent (10,943–98,469m^2 increase between 1984 and 2015 for different glaciers) and density of supraglacial pond and ice cliff networks. Pond and ice cliff networks expanded in both up- and down-glacier directions on different glaciers. We also documented the development of a slightly more pitted, terminus proximal, glacier surface where debris-covered glaciers have a linked supraglacial-proglacial hydrological network. The migration of supraglacial channels and associated incision (~10 m from 1984 to 2015) into the ice below may be the driver of topographic change here.

Overall, the changes in surface topography quantified in this study have important implications for both the hydrology and surface energy balance of those glaciers. The development of a glacier surface that is of greater relief is likely to lead to an increased contribution of the net radiative and turbulent heat fluxes to the overall energy balance at that glaciers surface. The development of a more pitted glacier surface will also increase accommodation space available for meltwater ponding, likely creating a positive feedback

between ponding, ice cliff backwasting, and topographic change. It is unlikely that this trajectory of topographic evolution will change given the sustained reduction of glacier surface gradients in response to glacier surface lowering and surface velocity reductions, which will all serve to precondition glacier surfaces for more ice cliff and supraglacial pond development. The areal coverage of pitted topography associated with pond expansion can reasonably be expected to expand on debris-covered glaciers not just in our study area but across the Himalaya, and should be accounted for in models of future glacier evolution that rely on parameterisations of surface energy balance to drive melt.

Declaration of competing interest

The authors declare that they have no known competing financial interests or personal relationships that could have appeared to influence the work reported in this paper.

Acknowledgements

OK was a recipient of a NERC SPHERES DTP PhD studentship (grant award NE/L002574/1). The Natural Environment Research Council Geophysical Equipment Facility (NERC GEF) is thanked for loaning Global Navigation Satellite Systems receivers and technical assistance under loan numbers 1050, 1058 and 1065. Dhananjay Regmi and Himalayan Research Expeditions are thanked for their support in fieldwork logistics. We thank Ian Howat for generating and sharing the 2 m WorldView DEMs. We thank Tobias Bolch for his input on an early version of the manuscript and support towards finalising the work.

Data availability

The glacier surface velocity data are available as part of the ITS_LIVE NASA MEaSUREs project (https://its-live.jpl.nasa.gov/). The 1984 DEMs and metric grids are available from the CEDA archive (http://archive.ceda.ac.uk/) under King_GlacierMetric, as is metadata providing further information about the derivation of the SMR metrics.

Appendix A. Supplementary data

Supplementary data to this article can be found online at https://doi.org/10.1016/j.geomorph.2020.107422.

References

Anderson, L.S., Anderson, R., 2016. Modeling debris-covered glaciers: response to steady debris deposition. Cryosphere 10, 1105–1124. https://doi.org/10.5194/tc-10-1105-2016.

Benn, D.I., Lehmkuhl, F., 2000. Mass balance and equilibrium-line altitudes of glaciers in high-mountain environments. Quaternary International 65-66, 15–29. https://doi.org/10.1016/S1040-6182(99)00034-8.

Benn, D.I., Bolch, T., Hands, K., Gulley, J., Luckman, A., Nichol-son, L.I., Quincey, D., Thompson, S., Toumi, R., Wiseman, S., 2012. Response of debris-covered glaciers in the Mount Everest re-gion to recent warming, and implications for outburst flood haz-ards. Earth-Sci. Rev. 114, 156–174.

Benn, D.I., Thompson, S., Gulley, J., Mertes, J., Luckman, A., Nicholson, L., 2017. Structure and evolution of the drainage system of a Himalayan debris-covered glacier, and its relationship with patterns of mass loss. Cryosphere 11, 2247–2264. https://doi.org/10.5194/tc-11-2247-2017.

Bolch, T., Buchroithner, M., Peters, J., Baessler, M., Bajracharya, S., 2008. Identification of glacier motion and potentially dangerous glacial lakes in the Everest region/Nepal using spaceborne imagery. Nat. Hazards Earth System Sci. 8, 1329–1340.

Bolch, T., Pieczonka, T., Benn, D.I., 2011. Multi-decadal mass loss of glaciers in the Everest area (Nepal Himalaya) derived from stereo imagery. Cryosphere 5, 349–358.

Bolch, T., Shea, J.M., Liu, S., Azam, F.M., Gao, Y., Gruber, S., et al., 2019. Status and change of the cryosphere in the extended Hindu Kush Himalaya Region. In: Wester, Philippus, Mishra, Arabinda, Mukherji, Aditi, Shrestha, Arun Bhakta (Eds.), The Hindu Kush Himalaya Assessment: Mountains, Climate Change, Sustainability and People. Springer International Publishing, pp. 209–255.

Brasington, J., Vericat, D., Rychkov, I., 2012. Modeling river bed morphology, roughness, and surface sedimentology using high resolution terrestrial laser scanning. Water Resour. Res. 48, W11519. https://doi.org/10.1029/2012WR012223.

Brun, F., Wagnon, P., Berthier, E., Shea, J.M., Immerzeel, W.W., Kraaijenbrink, P.D.A., Vincent, C., Reverchon, C., Shrestha, D., Arnaud, Y., 2018. Ice cliff contribution to the tongue-wide ablation of Changri Nup Glacier, Nepal, central Himalaya. Cryosphere 12, 3439–3457. https://doi.org/10.5194/tc-12-3439-2018.

Brun, F., Wagnon, P., Berthier, E., Jomelli, V., Maharjan, S.B., Shrestha, F., Kraaijenbrink, P.D.A., 2019. Heterogeneous influence of glacier morphology on the mass balance variability in High Mountain Asia. J. Geophys. Res.: Surf. 124, 1–15. https://doi.org/10.1029/2018JF004838.

Carrivick, J.L., Tweed, F.S., 2016. A global assessment of the societal impacts of glacier outburst floods. Glob. Planet. Chang. 144, 1–16. https://doi.org/10.1016/j.gloplacha.2016.07.001.

Chambers, J.R., Smith, M.W., Quincey, D.J., Carrivick, J.L., Ross, A.N., James, M.R., 2019. Glacial Aerodynamic roughness estimates: uncertainty, sensitivity, and precision in field measurements. J. Geophys. Res.: Earth Surf. 125. https://doi.org/10.1029/2019JF005167 e2019JF005167.

Dehecq, A., Gourmelen, N., Trouve, E., 2015. Deriving large-scale glacier velocities from a complete satellite archive: Application to the Pamir-Karakoram-Himalaya. Remote Sens. Environ. 162, 55–66. https://doi.org/10.1016/j.rse.2015.01.031.

Dehecq, N., Gourmelen, A., Gardner, S., Brun, F., Goldberg, D., Nienow, P.W., Berthier, E., Vincent, C., Wagnon, P., Trouvé, E., 2019. Twenty-first century glacier slowdown driven by mass loss in High Mountain Asia. Nat. Geosci. 12, 22–27.

Denby, B., Greuell, W., 2000. The use of bulk and profile methods for determining surface heat fluxes in the presence of glacier winds. J. Glaciol. 46, 445–452.

Haritashya, U.K., Kargel, J.S., Shugar, D.H., Leonard, G.J., Strattman, K., Watson, C.S., Shean, D., Harrison, S., Mandli, K.T., Regmi, D., 2018. Evolution and controls of large glacial lakes in the Nepal Himalaya. Remote Sensing 10, 798. https://doi.org/10.3390/rs10050798.

Herreid, S., Pellicciotti, F., 2020. The state of rock debris covering Earth's glaciers. Nature Geoscience https://doi.org/10.1038/s41561-020-0615-0.

Hock, R., 2005. Glacier melt: a review on processes and their modelling. Prog. Phys. Geogr. 29 (3), 362–391.

Immerzeel, W.W., Kraaijenbrink, P.D.A., Shea, J.M., Shrestha, A.B., Pellicciotti, F., Bierkens, M.F.P., de Jong, S.M., 2014. High-resolution monitoring of Himalayan glacier dynamics using unmanned aerial vehicles. Remote Sens. Environ. 150, 93–103.

Irvine-Fynn, T.D.L., Porter, P.R., Rowan, A.V., Quincey, D.J., Gibson, M.J., Bridge, J.W., Glasser, N.F., 2017. Supraglacial ponds regulate runoff from Himalayan debris-covered glaciers. Geophys. Res. Lett. 44, 11,894–11,904. https://doi.org/10.1002/2017GL075398.

King, J.C., Anderson, P.S., 1994. Heat and water vapour fluxes and scalar roughness lengths over an Antarctic ice shelf. Bound.-Layer Meteorol. 69, 101–121.

King, O., Dehecq, A., Quincey, D., Carrivick, J., 2018. Contrasting geometric and dynamic evolution of lake and land-terminating glaciers in the Central Himalaya. Glob. Planet. Chang. 167, 46–60.

King, O., Bhattacharya, A., Bhambri, R., Bolch, T., 2019. Glacial lakes exacerbate Himalayan glacier mass loss. Sci. Rep. 9, 18145. https://doi.org/10.1038/s41598-019-53733-x.

Kääb, A., Berthier, E., Nuth, C., Gardelle, J., Arnaud, Y., 2012. Contrasting patterns of early twenty-first-century glacier mass change in the Himalayas. Nature 488, 495–498.

Martin, E., Lejeune, Y., 1998. Turbulent fluxes above the snow surface. Ann. Glaciol. 26, 179–183.

Mattson, L.E., Gardner, J.S., Young, G.J., 1993. Ablation on Debris Covered Glaciers: An Example from the Rakhiot Glacier, Punjab, Himalaya. IAHS Publ. 218 (Symposium at Kathmandu, Nepal 1992 –Snow and Glacier Hydrology). pp. 289–296.

Maurer, J.M., Schaefer, J.M., Rupper, S., Corley, A., 2019. Acceleration of ice loss across the Himalayas over the past 40 years. Sci. Adv. 5, 6.

Miles, E.S., Willis .C., I, Arnold, N.S., Steiner, J., Pellicciotti, F., 2016. Spatial, seasonal and interannual variability of supraglacial ponds in the Langtang Valley, 1999-2013. J. Glaciol. 63 (237), 88–105. https://doi.org/10.1017/jog.2016.120.

Miles, E.S., Watson, C.S., Brun, F., Berthier, E., Esteves, M., Quincey, D.J., Miles, K.E., Hubbard, B., Wagnon, P., 2018. Glacial and geomorphic effects of a supraglacial lake drainage and outburst event, Everest region, Nepal Himalaya. Cryosphere 12, 3891–3905. https://doi.org/10.5194/tc-12-3891-2018.

Miles, K.E., Hubbard, B., Quincey, D.J., Miles, E.S., Irvine-Fynn, T.D.L., Rowan, A., 2019. Surface and subsurface hydrology of debris-covered Khumbu Glacier, Nepal, revealed by dye tracing. Earth and Planetary Science Letters 513, 176–186. https://doi.org/10.1016/j.epsl.2019.02.020.

Mölg, N., Bolch, T., Walter, A., Vieli, A., 2019. Unravelling the evolution of Zmuttgletscher and its debris cover since the end of the Little Ice Age. The Cryosphere 13, 1889–1909. https://doi.org/10.5194/tc-13-1889-2019.

Mölg, N., Fergusson, J., Bolch, T., Vieli, A., 2020. On the influence of debris cover on glacier morphology: how high-relief structures evolve from smooth surfaces. Geomorphology 357, 107092. https://doi.org/10.1016/j.geomorph.2020.107092.

Mukherjee, K., Bhattacharya, A., Pieczonka, T., Ghosh, S., Bolch, T., 2018. Glacier mass budget and climate reanalysis data indicatea climatic shift around 2000 in Lahaul-Spiti, western Himalaya. Climate Change 148 (1), 219–233. https://doi.org/10.1007/s10584-018-2185-3.

Nakawo, M., Iwata, S., Watanabe, O., Yoshida, M., 1986. Processes which Distribute Supraglacial Debris on the Khumbu Glacier, Nepal Himalaya. Ann. Glaciol. 8, 129–131. https://doi.org/10.3189/S0260305500001294.

Nicholson, L., Benn, D.I., 2006. Calculating ice melt beneath a debris layer using meteorological data. J. Glaciol. 52 (178), 463–470.

Noh, M.J., Howat, I.M., 2015. Automated stereo-photogrammetric DEM generation at high latitudes: Surface Extraction with TIN-based Search-space Minimization (SETSM) validation and demonstration over glaciated regions. Remote Sens. 52, 198–217.

Nuimura, T., Fujita, K., Yamaguchi, S., Sharma, R.R., 2012. Elevation changes of glaciers revealed by multitemporal digital elevation models calibrated by GPS survey in the Khumbu region, Nepal Himalaya, 1992–2008. J. Glaciol. 58, 648–656.

Nuth, C., Kääb, A., 2011. Co-registration and bias corrections of satellite elevation data sets for quantifying glacier thickness change. Cryosphere 5, 271–290.

Østrem, G., 1959. Ice melting under a thin layer of moraine, and the existence of ice cores in moraine ridges. Geogr. Ann. 41, 228–230.

Quincey, D., Richardson, S., Luckman, A., Lucas, R., Reynolds, J., Hambrey, M., Glasser, N., 2007. Early recognition of glacial lake hazards in the Himalaya using remote sensing datasets. Glob. Planet. Chang. 56, 137–152. https://doi.org/10.1016/j.gloplacha.2006.07.013.

Quincey, D., Luckman, A., Benn, D., 2009. Quantification of Everest region glacier velocities between 1992 and 2002, using satellite radar interferometry and feature tracking. J. Glaciol. 55, 596–606.

Quincey, D., Smith, M., Rounce, D., Ross, A., King, O., Watson, C., 2017. Evaluating morphological estimates of the aerodynamic roughness of debris-covered glacier ice. Earth Surf. Process Landf. 42, 2541–2553. https://doi.org/10.1002/esp.4198.

RGI Consortium, 2017. Randolph Glacier Inventory – A Dataset of Global Glacier Outlines: Version 6.0: Technical Report, Global Land Ice Measurements from Space, Colorado, USA. Digital Media. https://doi.org/10.7265/N5-RGI-60.

Rounce, D.R., Byers, A.C., Byers, E.A., McKinney, D.C., 2017. Brief communication: Observations of a glacier outburst flood from Lhotse Glacier, Everest area, Nepal. Cryosphere 11, 443–449. https://doi.org/10.5194/tc-11-443-2017.

Rounce, D.R., King, O., McCarthy, M., Shean, D.E., Salerno, F., 2018. Quantifying debris thickness of debris-covered glaciers in the Everest region of Nepal through inversion of a sub-debris melt model. J. Geophys. Res.: Earth Surf. 123, 1094–1115. https://doi.org/10.1029/2017JF004395.

Rowan, A.V., Egholm, D.L., Quincey, D.J., Glasser, N.F., 2015. Modelling the feedbacks between mass balance, ice flow and debris transport to predict the response to climate change of debris-covered glaciers in the Himalaya. Earth Planet. Sci. Lett. 430, 427–438.

Sakai, A., Nakawo, M., Fujita, K., 2002. Distribution characteristics and energy balance of ice cliffs on debris-covered glaciers, Nepal Himalaya. Arct. Antarct. Alp. Res. 34, 12–19. https://doi.org/10.2307/1552503.

Sakai, A., Nishimura, K., Kadota, T., Takeuchi, N., 2009. Onset of calving at supraglacial lakes on debris-covered glaciers of the Nepal Himalayas. J. Glaciol. 55 (193), 909–917. https://doi.org/10.3189/002214309790152555.

Salerno, F., Guyennon, N., Thakuri, S., Viviano, G., Romano, E., Vuillermoz, E., Cristofanelli, P., Stocchi, P., Agrillo, G., Ma, Y., Tartari, G., 2015. Weak precipitation, warm winters and springs impact glaciers of south slopes of Mt. Everest (central Himalaya) in the last 2 decades (1994–2013). The Cryosphere 9, 1229–1247. https://doi.org/10.5194/tc-9-1229-2015.

Smith, M.W., Carrivick, J.L., Quincey, D.J., 2016. Structure from motion photogrammetry in physical geography. Progress in Physical Geography: Earth and Environment 40 (2), 247–275. https://doi.org/10.1177/0309133315615805.

Somos-Valenzuela, M.A., Mckinney, D.C., Rounce, D.R., Byers, A.C., 2014. Changes in Imja Tsho in the Mount Everest region of Nepal. Cryosphere 8, 1661–1671.

Thakuri, A., Salerno, F., Bolch, T., Guyennon, N., Tartari, G., 2016. Factors controlling the accelerated expansion of Imja Lake, Mount Everest region. Nepal. Ann. Glaciol. 57, 71. https://doi.org/10.3189/2016AoG71A063.

Thakuri, S., Salerno, F., Smiraglia, C., Bolch, T., D'Agata, C., Viviano, G., Tartari, G., 2014. Tracing glacier changes since the 1960s on the south slope of Mt. Everest (central Southern Himalaya) using optical satellite imagery. Cryosphere 8, 1297–1315.

Thompson, S., Benn, D.I., Mertes, J., Luckman, A., 2016. Stagnation and mass loss on a Himalayan debris-covered glacier: processes, patterns and rates. J. Glaciol. 62 (233), 467–485. https://doi.org/10.1017/jog.2016.37.

Washburn, B., 1989. Mapping Mount Everest. Bull. Am. Acad. Arts Sci. 42 (7), 29–44. https://doi.org/10.2307/3824352.

Watson, C.S., Quincey, D.J., Carrivick, J.L., Smith, M.W., 2016. The dynamics of supraglacial ponds in the Everest region, central Himalaya. Glob. Planet. Chang. 142, 14–27.

Watson, C.S., Quincey, D.J., Carrivick, J.L., Smith, M.W., 2017a. Ice cliff dynamics in the Everest region of the central Himalaya. Geomorphology 278, 238–251 doi.org/10/106/j.geomorph.2016.11.017.

Watson, C.S., Quincey, D.J., Smith, M.W., Carrivick, J.L., Rowan, A.V., James, M.R., 2017b. Quantifying ice cliff evolution with multi-temporal point clouds on the debris-covered Khumbu Glacier, Nepal. J. Glaciol. 63 (241). https://doi.org/10.1017/jog.2017.47.